Mirror-based scanning wavefront-folding interferometer for universal coherence measurements

ATRI HALDER[1,*], HENRI PARTANEN[1,a], ALEKSI LEINONEN[1], MATIAS KOIVUROVA[2], TOMMI K. HAKALA[1], TERO SETÄLÄ[1], JARI TURUNEN[1], AND ARI T. FRIBERG[1]

[1] Institute of Photonics, University of Eastern Finland, P.O. Box 111, FI-80101 Joensuu, Finland
[2] Photonics Laboratory, Tampere University, P.O. Box 692, FI-33014 Tampere, Finland
[a] Current address: Dispelix Oy, Metsänneidonkuja 10, 02130 Espoo, Finland
[*] Corresponding author: atri.halder@uef.fi

Compiled July 6, 2020

We demonstrate a modification to the traditional prism-based wavefront-folding interferometer (WFI) that allows the measurement of spatial and temporal coherence, free of distortions and diffraction caused by the prism corners. In our modified system, the two prisms of the conventional system are replaced with six mirrors. The whole system is mounted on a linear XY-translation stage, with an additional linear stage in the horizontal arm. This system enables rapid and exact measurement of the full four dimensional degree of coherence, even for relatively weak signals. The capabilities of our system are demonstrated by measuring the spatial coherence of two inhomogeneous and non-Schell model light sources with distinct characteristics.

http://dx.doi.org/10.1364/ao.XX.XXXXXX

Coherence is one of the most fundamental properties of light, since it largely defines the features and behaviour of all light fields [1]. As interference phenomena are strongly dependent on the correlations of superposed fields, the spatial and temporal coherence measurements become evidently important in order to characterize the properties of newly developed light sources. These include, e.g., arbitrary non-uniform partially coherent light sources, nano-lasers, and non-linear sources. Spatial coherence has traditionally been measured using Young's double pinhole interferometer [1]. However, this method has two downsides: speed and light efficiency, as light is sampled by two tiny pinholes at a time. Young's method has been improved upon [2–4], but the main deficiencies still remain. Multiple alternative solutions for spatial coherence measurement have been proposed, such as ones based on shadows [5], Mach-Zehnder interferometer [6], gratings [7], masks [8], fiber optics [9], and intensity correlation [10]. Although being improvements to the original Young's interferometer, none of the aforementioned methods are able to conveniently and rapidly measure the full four dimensional spatial coherence function, nor both spatial and temporal coherence with the same setup. Having several distinct measurement setups for the characterization of a single source may occupy significant lab space and be impractical. Thus a more universal arrangement is desirable.

Wavefront-folding interferometers (WFIs), which measure several point pairs at once [11–15] also improve upon the traditional Young's setup. In the original configuration, WFIs consist of crossed right angle retro-reflecting prisms, allowing the measurement of spatial coherence of Schell-model fields (coherence as a function of coordinate difference). The shortcomings of this type of WFIs also include the obscuring shadow caused by the prism corners, and the polarization modulation due to the total internal reflections inside the glass. These effects can cause significant issues with weak intensities and in the measurement of non-uniformly polarized light. One way to overcome the shadowing problem is to expand the incident beam sufficiently, which may not always be practical. An alternative way is to change the prisms in the WFI to something else entirely.

Recently, we introduced a mirror-based WFI that flipped the beam in one direction [16], allowing coherence measurements between two arbitrary points in one dimension. Here we introduce a system that folds the beam along both x- and y-axes, thus, allowing for the measurement of the full four dimensional coherence function $\mu(\bar{x}, \Delta x; \bar{y}, \Delta y)$ in mean $(\bar{x}, \bar{y})$ and difference $(\Delta x, \Delta y)$ coordinates, by shifting the whole WFI (or the light source) in the x- and y-directions. Additionally, by using mirrors we can negate the obstruction caused by prism corners and reflections from the front surfaces of the prisms completely, as well as make the setup almost completely polarization insensitive. The proposed system also allows the measurement of temporal coherence by adjusting the optical path length difference Δz_e (or, equivalently, the time delay Δt), in addition to transverse spatial coordinates. In the present study we demonstrate the capabilities of our setup by measuring the spatial coherence of two light sources: a partially coherent and partially polarized multi-mode HeNe laser, and a multi-mode broad-area laser diode. Before the demonstrations we present our setup, and give a brief overview of the theory.

The employed WFI system, depicted in Fig. 1, consists of two interferometer arms, where one folds the beam in vertical and the other in horizontal direction. The 'UEF' text visualizes how the beam handedness gets folded inside the system. The whole system includes six mirrors divided into two arms, with four in

the vertical arm and two in the horizontal one. The two mirrors in the horizontal arm are mounted on a linear translation stage, which are used to adjust the optical path length difference Δz_e between the two arms, enabling the measurement of temporal coherence. Both arms include motorized shutters in order to block the beams when needed. The whole system is mounted on an XY-translation stage to enable scanning without moving the light source itself. Scanning the measurement system in either direction corresponds to a shear in the mean coordinate of the measured beam. Tilt of all mirrors may be adjusted independently to change the angle between the beams and the position where they cross, which modulates the observed fringe pattern. The second beam-splitter (or combiner) has two outputs. This allows us to place the camera detector at output 1, where we can form the image of the source, while simultaneously study far-field of the beam at output 2 using an additional Fourier-transform lens.

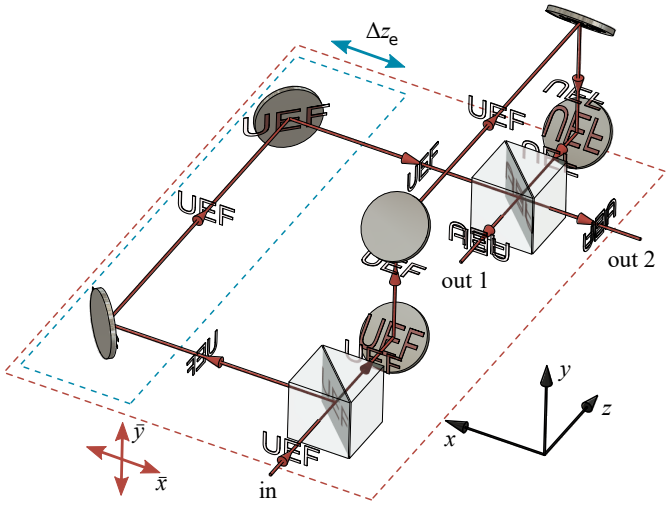

Fig. 1. Skeleton of the measurement system, where the 'UEF' text visualizes how the beam handedness gets folded by the mirrors in the system. Here Δz_e is the path length difference, (x, y, z) represent the laboratory coordinates, and $(\bar{x}, \bar{y})$ indicates the relevant scanning directions.

Due to the similarity between the traditional WFI and our mirror-based system, we only present the most crucial formulae; for complete derivation we guide the reader to [16]. The expression for the spectral field with frequency ω, at the rotated detector frame of reference (x_d, y_d) with respect to the input frame (x, y) is

$$E(x_d, y_d; \omega) = \frac{1}{2}\{E_0(x_1, y_2; \omega)\exp[iC_x(\omega)x_d] + E_0(x_2, y_1; \omega)\exp[-iC_y(\omega)y_d]\exp[i\phi(\omega)]\}, \quad (1)$$

where $E_0(x, y; \omega)$ is the input field. Additionally, $\phi(\omega) = 2\Delta z_e\omega/c$, with Δz_e being the shift from the equal-path position, as depicted in Fig 1. The terms $C_x(\omega) = (\omega/c)\sin\alpha_x$ and $C_y(\omega) = (\omega/c)\sin\alpha_y$ account for the beam tilts, α_x and α_y, in x and y directions due to relative mirror alignment; we assume that each arm tilts the beam only along one axis. Furthermore, $x_1 = \bar{x} - \Delta x/2$, and $y_1 = \bar{y} - \Delta y/2$ are the sheared coordinates, whereas $x_2 = \bar{x} + \Delta x/2$, and $y_2 = \bar{y} + \Delta y/2$ are the sheared *and* folded transverse coordinates. In the theoretical formulation, we assume the input beam as being perfectly collimated, and as such its spatial coherence function remains the same upon propagation. In the experimental case this is not strictly true, although the Rayleigh range can be much longer than the WFI size. Instead, in the experiment, it is possible to image the source plane or any propagation plane onto the camera detector plane at the output (which we have done) thus ignoring diffraction effects. Note that, at any fixed $(\bar{x}, \bar{y})$ position of the WFI, the detector measures coherence along difference coordinates $(\Delta x, \Delta y)$. Scanning the device shears the measurement over the average coordinates $(\bar{x}, \bar{y})$, thus allowing the measurement of the four-dimensional coherence function.

Utilizing Eq. (1), an expression for the spectral density at the detector can be written as

$$S(x_d, y_d) = \frac{1}{4}[S_0(x_1, y_2) + S_0(x_2, y_1)] + \frac{1}{2}\sqrt{S_0(x_1, y_2)S_0(x_2, y_1)} \times |\mu_0(x_1, y_2, x_2, y_1)|\cos[\Phi_0(x_1, y_2, x_2, y_1) - \beta], \quad (2)$$

where we have left the ω dependence implicit for brevity. In the above expression, $\Phi_0(x_1, y_2, x_2, y_1)$ is the phase of the complex degree of coherence of the incident field, $\mu_0(x_1, y_2, x_2, y_1)$, and $\beta = C_x x_d + C_y y_d - \phi$. Therefore, the visibility, V, of the fringes can also be written in the form

$$V(x_d, y_d) = \frac{2\sqrt{S_0(x_1, y_2)S_0(x_2, y_1)}}{S_0(x_1, y_2) + S_0(x_2, y_1)}|\mu_0(x_1, y_2, x_2, y_1)|. \quad (3)$$

The absolute value and the phase of the complex degree of coherence can be retrieved from the measured fringe visibility and position data.

In the space-time domain, a presentation for the modulated interference pattern (derived from the mutual coherence function in [16]) is

$$I(x_d, y_d) = \frac{1}{4}[I_0(x_1, y_2) + I_0(x_2, y_1)] + \frac{1}{2}\sqrt{I_0(x_1, y_2)I_0(x_2, y_1)}|\gamma_0[x_1, y_2, x_2, y_1; \tau(x_d, y_d) - \tau]| \times \cos\{\psi_0[x_1, y_2, x_2, y_1; \tau(x_d, y_d) - \tau] - \omega_0[\tau(x_d, y_d) - \tau]\}, \quad (4)$$

where $\psi_0[x_1, y_2, x_2, y_1; \tau(x_d, y_d) - \tau]$ is the phase of the temporal complex degree of coherence $\gamma_0[x_1, y_2, x_2, y_1; \tau(x_d, y_d) - \tau]$, and ω_0 is the carrier frequency. Additionally, $\tau(x_d, y_d) = 2[x_d\sin(\alpha_x) + y_d\sin(\alpha_y)]/c$ is the position-dependent time delay due to the relative tilt between the interfering wavefronts, and $\tau = 2\Delta z_e/c = \phi(\omega)/\omega$ is the time delay due to optical path difference. The visibility of the temporal domain fringe pattern is given by

$$V(x_d, y_d) = \frac{2\sqrt{I_0(x_1, y_2)I_0(x_2, y_1)}}{I_0(x_1, y_2) + I_0(x_2, y_1)} \times |\gamma_0[x_1, y_2, x_2, y_1; \tau(x_d, y_d) - \tau]|. \quad (5)$$

In the experiments reported below the measurements were carried out with quasi-monochromatic light sources, for which the coherence length was much larger than the position dependent time delay $\tau(x, y)$. Hence, we essentially measure the equal-time degree of coherence of a narrowband field, which coincides with the spectral degree of coherence [17], and we will use the spectral domain formulation for the remainder of the article.

In each measurement we capture three intensity profiles: $I(x_d, y_d)$ with both arms open, $I_1(x_d, y_d) = I_0(x_1, y_2)$ and $I_2(x_d, y_d) = I_0(x_2, y_1)$ with only one arm open at a time. In

addition, we capture a dark frame with both arms blocked to account for possible stray light. To compensate for the non-homogeneous intensity profile of the beams, we normalize the fringes with

$$I_{\text{norm}} = \frac{I - I_1 - I_2}{2\sqrt{I_1 I_2}}, \tag{6}$$

where the resulting I_{norm} is real valued with values between $[-1, 1]$. The absolute value of the degree of coherence is contained in the amplitude of the I_{norm} fringes, whereas the phase information is encoded into the position of the fringes.

In order to extract the complex-valued degree of coherence we remove the carrier frequency defined by the fringe period, by taking a two-dimensional Fourier transform $\mathcal{F}[I_{\text{norm}}]$ and applying some simple Fourier signal processing. Since I_{norm} is real valued, its Fourier transform features two side maxima, representing the positive and negative frequencies. The center zero frequency peak is removed (apart for some residual noise) by Eq. (6). We remove the negative frequencies by cropping one of the peaks and inverse Fourier transforming back to the spatial domain. Moreover, to maintain correct scaling the recovered signal needs to be multiplied by two. This results in a complex valued degree of coherence function, $\mu(\bar{x}, \Delta x; \bar{y}, \Delta y)$, where the center coordinates $\bar{x}$ and $\bar{y}$ are fixed to the mirroring point of the WFI, which we may freely scan by moving the whole WFI setup (or the light source being measured) in $\bar{x}$ and $\bar{y}$ directions. By scanning the WFI in one direction we detect the three dimensional $\mu(\bar{x}, \Delta x; \bar{y}, \Delta y)$ where the value of either $\bar{x}$ or $\bar{y}$ is fixed, depending on the scanning direction. If we scan the WFI sequentially in both directions we can measure the full four dimensional coherence function. As this type of data is naturally challenging to present, we only show 2D cross-sections of it.

Next we move on to the coherence measurements of two lasers: a partially coherent and partially polarized multi-mode HeNe laser (Lasos LGK 7621 MM, $\lambda = 632.8$ nm, 5 mW), and a multi-mode broad-area laser diode (Opnext HL6388MG, $\lambda = 637$ nm, 250 mW) for which the coherence was measured at three different values of the driving current. We scanned the multi-mode HeNe laser horizontally ($\bar{x}$) with the WFI. Centered measurement results, with $\mu(0, \Delta x; 0, \Delta y)$, are depicted in Fig. 2, whereas Fig. 3 shows the cross-section of the full $\bar{x}$ scan, i.e., $\mu(\bar{x}, \Delta x; 0, 0)$.

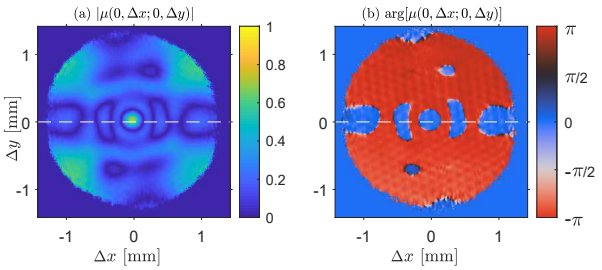

Fig. 2. Single measurement of the multi-mode HeNe laser for a single value $\bar{x} = 0$. (a) Retrieved absolute value of complex valued spatial degree of coherence function $\mu(0, \Delta x; 0, \Delta y)$. (b) Phase $\arg[\mu(0, \Delta x; 0, \Delta y)]$. For the effect of scanning the center coordinate $\bar{x}$ see Visualization 1.

From Fig. 2(a) it is evident that the coherence has modulation along both x- and y-directions. In addition, the middle spot indicates that the coherence length is short in both directions. Figure. 2(b) indicates that the phase is mainly binary, or that the coherence function is almost real valued, modulated only by a spherical phase front. See Visualisation 1 for the effect of scanning $\bar{x}$ and a description of the related experimental procedures. The location of the cross-section depicted in Fig. 3 is indicated by the white dashed line in Fig. 2. Absolute value of the degree of coherence in Fig. 3(a) has several side maxima, while its phase in Fig. 3(b) again features π phase shifts modulated by a spherical phase front.

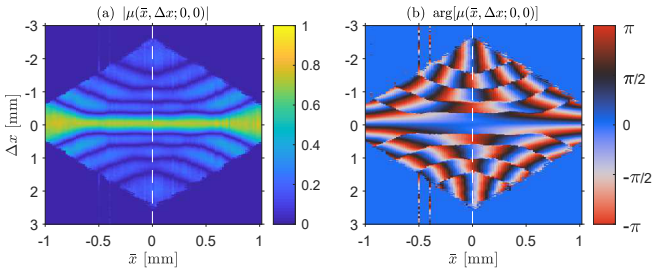

Fig. 3. Measured complex valued $\mu(\bar{x}, \Delta x; 0, 0)$ of the multi-mode HeNe laser. (a) Amplitude. (b) Phase.

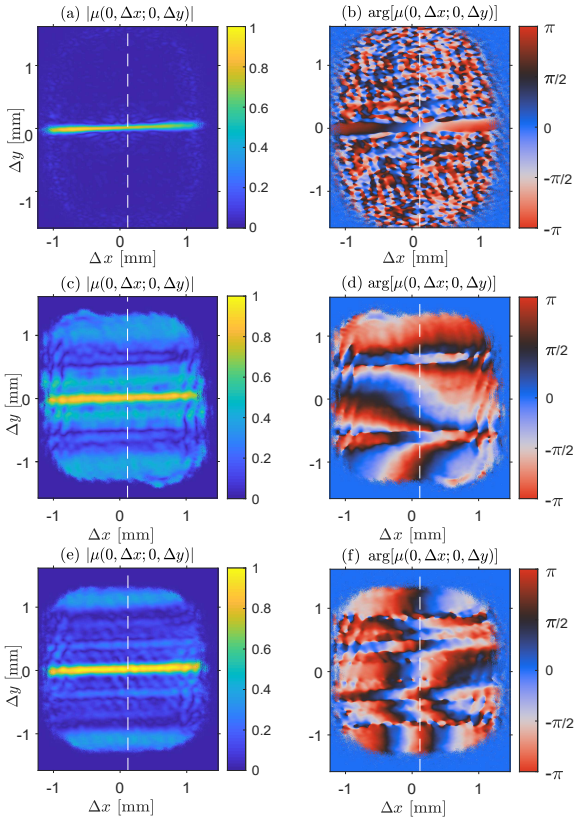

Fig. 4. Same as Fig. 2, but for the multi-mode broad-area laser diode at (a, b) 200 mA, (c, d) 280 mA, and (e, f) 420 mA driving current. For the effect of scanning the center coordinate $\bar{y}$ for 420 mA driving current see Visualization 2.

Next we measured the multi-mode broad-area laser diode at three different driving currents $i = 200$ mA, $i = 280$ mA, and $i = 420$ mA. We have previously characterized lasers of this type using Young's interferometer [18]. The beam was collimated using a $10\times$ magnifying microscope objective. The image of

the diode end facet was slightly defocused on the WFI camera detector; a perfectly focused image would be a narrow vertical line. In this measurement we scanned the WFI vertically in $\bar{y}$ direction, contrary to the case of the horizontal scan with HeNe laser. Figure 4 contains information similar to Fig. 2, but for the laser diode.

The data presented in Fig. 4 delineates that the diode beam is almost fully coherent in the horizontal x-direction and coherence modulation only exists in the vertical y-direction. This is explained by the diode resonator shape: it is narrow in the x-direction and allows essentially only one resonator mode, leading to high coherence, while the resonator is much wider in y-direction resulting in more modes and, thus, a decrease in the degree of coherence. Cross-sections similar to Fig. 3 are depicted in Fig. 5. Note that for this diode we present $\mu(0,0;\bar{y},\Delta y)$ instead of $\mu(\bar{x},\Delta x;0,0)$ for the HeNe laser because of the difference in scanning direction. See Visualisation 2 for the scanning of $\bar{y}$ in the case of 420 mA driving current.

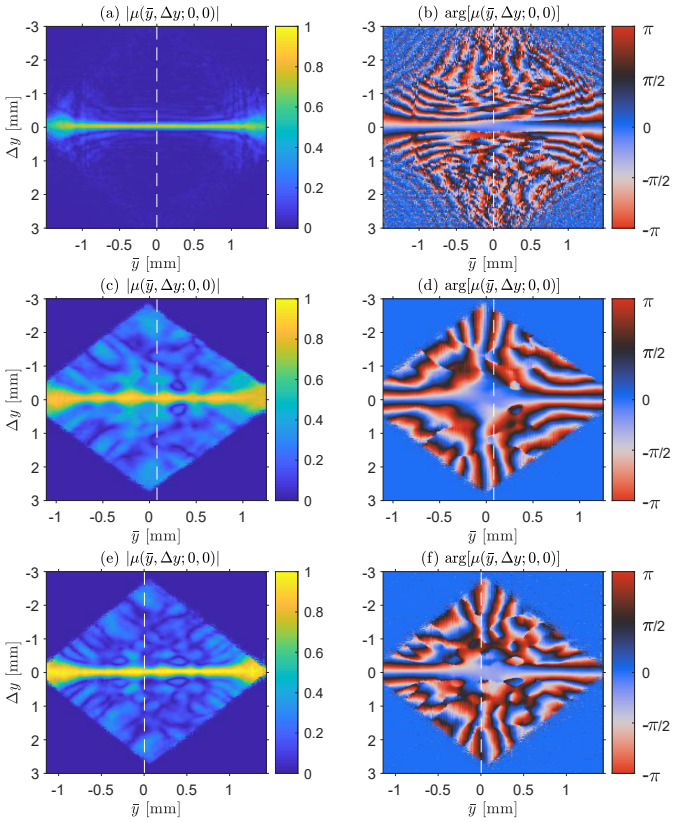

Fig. 5. Measured complex valued $\mu(0,0;\bar{y},\Delta y)$ of the multimode laser diode at three driving currents, 200 mA on top row (a) and (b), 280 mA at middle row (c) and (d), 420 mA at bottom row (e) and (f). The absolute value of μ is shown at left side in (a), (c) and (e), and the phase at right side (b), (d), and (f).

At the lowest current we measured, 200 mA, the diode is not yet lasing and coherence is low, indicated by the narrow lines in Figs. 4(a) and 5(a), as well as the noisy phase profiles in Figs. 4(b) and 5(b). At this driving current, the diode is working essentially as an LED. The diode starts to lase at about 280 mA, and only a few resonator modes are present, as the coherence function is rather wide and does not have many features. More modes exist at the highest measured current, 420 mA, indicated by more and smaller features of the coherence function.

To conclude, we have introduced and demonstrated a new type of WFI, further expanding on existing designs. Our previous design [16] already negated the harmful effects caused by the prism corners in the traditional WFI [12, 19]. In the present study we consider a system with the capability to perform universal coherence measurements in both spatial and temporal domains, with the possibility to measure the full four dimensional spatial coherence function. This versatility and robustness in the setup, that can be easily automated, makes this solution particularly beneficial for coherence measurements. Here we have only demonstrated the system in spatial domain but the device is applicable in the temporal domain as well. Some additional features of our setup include the possibility for lensless imaging and generation of perfect specular and anti-spacular beams [19], which will be reported separately. Although the device negates most of the problems in spatial coherence measurements, some issues may still be caused by possible imperfections in the mirrors or beam splitters, but they are less severe than with the traditional prism based WFI. Also, as is true in all optical measurements, temperature fluctuations and stray light from outside of the setup may cause problems. These can be negated by confining the system inside protective casing, but such problems are mostly limited to low signal sources.

ACKNOWLEDGEMENTS

This work is part of the Academy of Finland's Flagship programme Photonics Research and Innovation (PREIN, 320166, 320165). Additional funding was provided by Academy of Finland projects 322002, and 308393.
Disclosures: The authors declare no conflicts of interest.

REFERENCES

1. L. Mandel and E. Wolf, *Optical Coherence and Quantum Optics*, Cambridge University (1995).
2. E. Tervonen, J. Turunen, and A. T. Friberg, Appl. Phys. B **49**, 409 (1989).
3. M. Santarsiero and R. Borghi, Opt. Lett. **31**, 861 (2006).
4. K. Saastamoinen, J. Tervo, J. Turunen, P. Vahimaa, and A. T. Friberg, Opt. Express **21**, 4061 (2013).
5. J. K. Wood, A. K. Sharma, S. Cho, T. G. Brown, and M. A. Alonso, Opt. Lett. **39**, 4927 (2014).
6. C. Hitzenberger, M. Danner, W. Drexler, and A. Fercher, J. Mod. Opt. **46**, 1763 (1999).
7. M. Koivurova, H. Partanen J. Turunen, and A. T. Friberg, Appl. Opt. **56**, 5216 (2017).
8. Y. Mejía and A. González, Opt. Commun. **273**, 428 (2007).
9. B. L. Anderson and P. L. Fuhr, Opt. Eng. **32**, 926 (1993).
10. Z. Huang, Y. Chen, F. Wang, S. A. Ponomarenko, and Y. Cai, Phys. Rev. Applied **13**, 044042 (2020).
11. H. W. Wessely and J. O. Bolstad, J. Opt. Soc. Am. **60**, 678 (1970).
12. Q. He, J. Turunen, and A. T. Friberg, Opt. Commun. **67**, 245 (1988).
13. J. B. Breckinridge, Appl. Opt. **11**, 2996 (1972).
14. H. Arimoto and Y. Ohtsuka, Opt. Lett. **22**, 958 (1997).
15. M. Guo and D. Zhao, Opt. Express **27**, 8581 (2018).
16. M. Koivurova, H. Partanen, J. Lahyani, N. Cariou, J. Turunen, Opt. Express **27**, 7738 (2019).
17. H. Partanen, B. J. Hoenders, A. T. Friberg and T. Setälä, J. Opt. Soc. Am. A **35**, 1379 (2018).
18. H. Partanen, J. Turunen, and J. Tervo, Opt. Lett. **39**, 1034 (2014).
19. H. Partanen, N. Sharmin, J. Tervo, and J. Turunen, Opt. Express **23**, 28718 (2015)

REFERENCES

1. L. Mandel and E. Wolf, *Optical Coherence and Quantum Optics*, Cambridge University (1995).
2. E. Tervonen, J. Turunen, and A. T. Friberg, “Transverse laser-mode structure determination from spatial coherence measurements: experimental results,” Appl. Phys. B **49**, 409–414 (1989).
3. M. Santarsiero and R. Borghi, “Measuring spatial coherence using a reversed-wavefront Young’s interferometer,” Opt. Lett. **31**, 861 (2006).
4. K. Saastamoinen, J. Tervo, J. Turunen, P. Vahimaa, and A. T. Friberg, “Spatial coherence measurement of polychromatic light with modified Young’s interferometer,” Opt. Express. **21**, 4061 (2013).
5. J. K. Wood, A. K. Sharma, S. Cho, T. G. Brown, and M. A. Alonso, “Using shadows to measure spatial coherence,” Opt. Lett. **39**, 4927 (2014).
6. C. Hitzenberger, M. Danner, W. Drexler, and A. Fercher, “Measurement of the spatial coherence of superluminescent diodes,” J. Mod. Opt. **46**, 1763 (1999).
7. M. Koivurova, H. Partanen J. Turunen, and A. T. Friberg, “Grating interferometer for light-efficient spatial coherence measurement of arbitrary sources,” Appl. Opt. **56**, 5216 (2017).
8. Y. Mejía and A. González, “Measuring spatial coherence by using a mask with multiple apertures,” Opt. Commun. **273**, 428 (2007).
9. B. L. Anderson and P. L. Fuhr, “Twin-fiber interferometric method for measuring spatial coherence,” Opt. Eng. **32**, 926 (1993).
10. Z. Huang, Y. Chen, F. Wang, S. A. Ponomarenko, and Y. Cai, “Measuring complex degree of coherence of random light fields with generalized Hanbury Brown–Twiss experiment,” Phys. Rev. Applied **13**, 044042 (2020).
11. H. W. Wessely and J. O. Bolstad, “Interferometric technique for measuring the spatial-correlation function of optical radiation fields,” J. Opt. Soc. Am. **60**, 678 (1970).
12. Q. He, J. Turunen, and A. T. Friberg, “Propagation and imaging experiments with Gaussian Schell-model beams,”Opt. Commun. **67**, 245 (1988).
13. J. B. Breckinridge, “Coherence interferometer and astronomical applications,” Appl. Opt. **11**, 2996 (1972).
14. H. Arimoto and Y. Ohtsuka, “Measurements of the complex degree of spectral coherence by use of a wave-front-folded interferometer,” Opt. Lett. **22**, 958 (1997).
15. M. Guo and D. Zhao, "Polarization properties of stochastic electromagnetic beams modulated by a wavefront-folding interferometer", Opt. Express **27**, 8581 (2018).
16. M. Koivurova, H. Partanen, J. Lahyani, N. Cariou, J. Turunen, “Scanning wavefront folding interferometers,” Opt. Express. **27**, 7738 (2019).
17. H. Partanen, B. J. Hoenders, A. T. Friberg and T. Setälä,“Young’s interference experiment with electromagnetic narrowband light,” J. Opt. Soc. Am. A **35**, 1379 (2018).
18. H. Partanen, J. Turunen, and J. Tervo, “Coherence measurement with digital micromirror device,” Opt. Lett. **39**, 1034 (2014).
19. H. Partanen, N. Sharmin, J. Tervo, and J. Turunen, “Specular and antispecular light beams,” Opt. Express **23**, 28718 (2015).